C. R. Physique 15 (2014) 18–29

Contents lists available at ScienceDirect

Comptes Rendus Physique

www.sciencedirect.com

Quasicrystals / Quasicristaux

About the atomic structures of icosahedral quasicrystals

Structures atomiques des phases icosaédriques: une courte chronologie

Marianne Quiquandon *, Denis Gratias

LEM UMR 104 CNRS/ONERA, ONERA, BP 72, 29, avenue de la Division-Leclerc, 92322 Châtillon cedex, France

ARTICLE INFO

Article history:
Available online 6 December 2013

Keywords:
Complex intermetallic alloys
Quasicrystals
Icosahedral phases
N-dim crystallography

Mots-clés :
Alliages intermétalliques complexes
Quasicristaux
Phases icosaédriques
Cristallographie *N*-dimensionnelle

ABSTRACT

This paper is a survey of the crystallographic methods that have been developed these last twenty five years to decipher the atomic structures of the icosahedral stable quasicrystals since their discovery in 1982 by D. Shechtman. After a brief recall of the notion of quasiperiodicity and the natural description of $\mathbb{Z}$-modules in 3-dim as projection of regular lattices in $N > 3$-dim spaces, we give the basic geometrical ingredients useful to describe icosahedral quasicrystals as irrational 3-dim cuts of ordinary crystals in 6-dim space. Atoms are described by atomic surfaces (ASs) that are bounded volumes in the internal (or perpendicular) 3-dim space and the intersections of which with the physical space are the actual atomic positions. The main part of the paper is devoted to finding the major properties of quasicrystalline icosahedral structures. As experimentally demonstrated, they can be described with a surprisingly few high symmetry ASs located at high symmetry special points in 6-dim space. The atomic structures are best described by aggregations and intersections of high symmetry compact interpenetrating atomic clusters. We show here that the experimentally relevant clusters are derived from one generic cluster made of two concentric triacontahedra scaled by τ and an external icosidodecahedron. Depending on which ones of the orbits of this cluster are eventually occupied by atoms, the actual atomic clusters are of type Bergman, Mackay, Tsai and others....

RÉSUMÉ

Cet article traite des méthodes cristallographiques développées au cours de ces 25 dernières années pour analyser et comprendre les structures atomiques des quasicristaux icosaédriques depuis leur découverte par D. Shechtman en avril 1982. Après un bref rappel des notions de $\mathbb{Z}$-modules dans l'espace vus comme projections irrationnelles de réseaux réguliers dans des espaces euclidiens à $N > 3$ dimensions, nous donnons les ingrédients géométriques utiles à la description des quasicristaux comme coupes irrationnelles de cristaux dans un espace euclidien de dimension 6. Les atomes sont décrits par des surfaces atomiques, volumes bornés dans l'espace interne (ou perpendiculaire), dont les intersections avec l'espace physique définissent les positions atomiques. L'essentiel de cet article est consacré à la détermination des propriétés principales qu'ont les quasicristaux icosaédriques engendrés par un petit nombre de surfaces atomiques de haute symétrie, localisées sur des points spéciaux de la structure à six dimensions, comme le suggèrent tous les résultats expérimentaux. On s'aperçoit alors que les structures atomiques sont bien décrites par l'agrégation et l'interpénétration d'amas atomiques compacts de haute symétrie. Ils sont tous dérivés d'un modèle générique constitué de deux triacontaèdres

* Corresponding author.
E-mail addresses: marianne.quiquandon@onera.fr (M. Quiquandon), denis.gratias@onera.fr (D. Gratias).

1631-0705/$ – see front matter
http://dx.doi.org/10.1016/j.crhy.2013.09.008

concentriques de tailles dans le rapport τ entourés d'un icosidodécaèdre extérieur. Selon les orbites de cet amas générique qui sont ou non occupées par des atomes, on obtient les différents types d'amas rencontrés usuellement dans les structures intermétalliques complexes, parmi lesquels les amas de type Bergman, Mackay, Tsai et autres....

1. Introduction

Quasicrystals have been discovered by D. Shechtman in a rapidly solidified (Al,Mn) alloy [1,2] by means of electron microscopy observations, as those shown in Fig. 1. This astonishing discovery has been made possible because electron microscopy allowed him to observe 3D single grain diffractions of the precipitates (Fig. 1), where he could recognize at once the long-range order of these solids together with their overall non-crystallographic icosahedral symmetry (shown in Fig. 2).

Soon after Shechtman's first observations, X-ray powder and neutron diffraction experiments were performed at NIST (Gaithersburg MD, USA)—and confirmed at CECM-CNRS (Vitry, France)—which exhibited well-defined sharp peaks like usual crystals, but could not be indexed in a way coherent with the icosahedral symmetry [3–5] observed with the electron microscope. The first explanations came very soon at the end of 1984, with the notion of *quasiperiodicity* and the derived term *quasicrystals* introduced by D. Levine and P.A. Steinhardt in a famous seminal paper [6]. Immediately after, in early 1985, came the famous *cut-and-project method* independently found by M. Duneau and A. Katz [7–9], P.A. Kalugin, A.Y. Kitaev and L.S. Levitov [10,11], and V. Elser [12–14].

The key idea that solved the apparent paradox of a *crystal with a non-crystallographic symmetry* is the fact that a quasiperiodic object in a space of dimension d is a d-dimensional cut of an $N > d$-dimensional *periodic object* along an orientation that is incommensurate with the periods of the object: this new icosahedral phase has been quickly recognized as a quasiperiodic crystal, a *quasicrystal* as quoted by Levine and Steinhardt [6], which could indeed be formally described by a *periodic* object in a six-dimensional space. Hence, the first structural models (see, for instance, [16–18]) already appeared at the beginning of 1986 based on this description, as it will be discussed here.

2. Basics

As experimentally observed very early, the intense X-rays and neutrons powder diffraction peaks of the icosahedral phases can all be labeled using one positive integer number N: all strong peaks being located at reciprocal wave vectors scaling like $|q|^2 \sim N + \lfloor N\tau \rfloor \tau$, where τ is the golden mean $\tau = (1+\sqrt{5})/2$. This extraordinary property could be eventually explained because, as demonstrated in [19], the electron diffraction patterns can be indexed in a way similar to that used for cubic crystals, *but* using *two* indices per cubic direction instead of *one*: $Q = (h + h'\tau, k + k'\tau, \ell + \ell'\tau)$, with $h, h', k, k', \ell, \ell' \in \mathbb{Z}$. This fact is a direct consequence of the icosahedral structures being 3D cuts irrationally oriented with respect to the periods of periodic objects in an Euclidean space $\mathbf{E}^6$ of dimension 6. The orientation of the physical space in the 6D space is obtained by analyzing the character table (displayed in Fig. 3) of the hemihedral group 235 of the regular icosahedron. It shows that the smallest *integer* representation of the group containing the representation Γ_3—which corresponds to the realization of 235 in the physical space—is of dimension 6 and is the combination of the representations Γ_3 and $\Gamma_{\bar{3}}$ that are arithmetically conjugated.[1] This leads to defining the 6D space as the product of two orthogonal subspaces, each of dimension 3, which are noted $\mathbf{E}_\parallel$ and $\mathbf{E}_\perp$:

$$\mathbf{E}^6 = \mathbf{E}_\parallel \oplus \mathbf{E}_\perp$$

The subspace $\mathbf{E}_\parallel$ corresponds to the representation Γ_3 and is the physical space designated here as *parallel space*; the subspace $\mathbf{E}_\perp$, complementary to the previous one, corresponds to the representation $\Gamma_{\bar{3}}$ and is the internal space, designated here as *perpendicular space*.

As illustrated in Fig. 3, the cut (and project) method, under its simplest form, consists in copying atomic surfaces σ, that are bounded volumes parallel to $\mathbf{E}_\perp$ discussed in Section 2.3, on the nodes of the N-dimensional lattice Λ, to form a periodic set $\Sigma = \bigcup_{\lambda\in\Lambda} \sigma_\lambda$, and cut it by the subspace $\mathbf{E}_\parallel$. The intersection points are the actual localizations of the real atoms.

2.1. Indexation

Going back and forth between the two mutually orthogonal 3D subspaces $\mathbf{E}_\parallel$ and $\mathbf{E}_\perp$ in the 6D space $\mathbf{E}^6$ is easily performed by using the change of basis matrix $\widehat{\boldsymbol{M}}$ defined as follows. Designating $\{|\alpha\rangle\}$ as the 3D orthonormal basis of $\mathbf{E}_\parallel$ and by $\{|\bar{\alpha}\rangle\}$ the one of $\mathbf{E}_\perp$, we designate by $\langle\alpha|i\rangle$ and $\langle\bar{\alpha}|i\rangle$ the projections of the canonical 6D basis $\{|i\rangle; i = 1, 6\}$ in the two

[1] Two representations are arithmetically conjugated if the sum of theirs characters are integers.

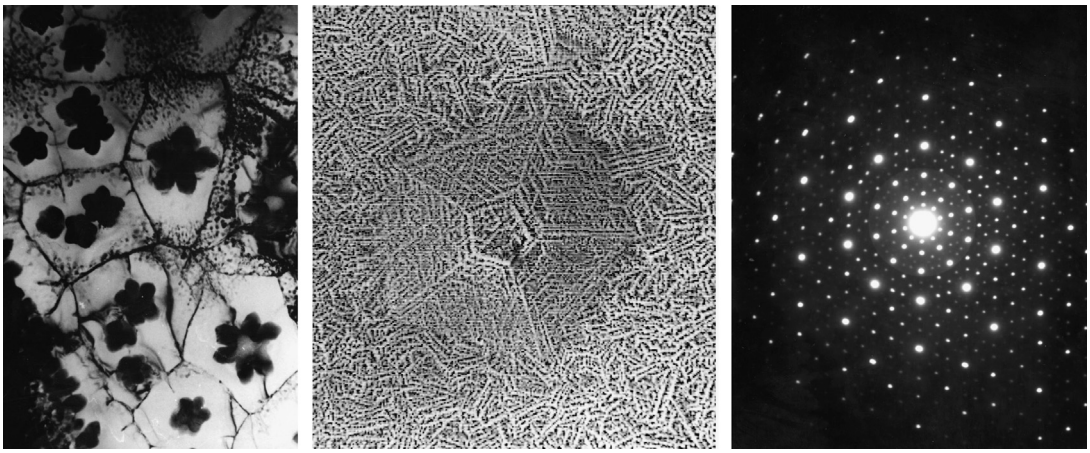

Fig. 1. Early observations of icosahedral quasicrystals in the (Al,Mn) and (Al,Mn,Si) metallic systems. Left: conventional electron micrograph of a rapidly quenched Al_6Mn alloy (courtesy of R. Portier et al. [4]); middle: scanning electron microscopy image of a rapidly quenched AlMnSi alloy; right: the corresponding electron diffraction diagram (courtesy of A. Quivy and J. Devaud-rzepsky).

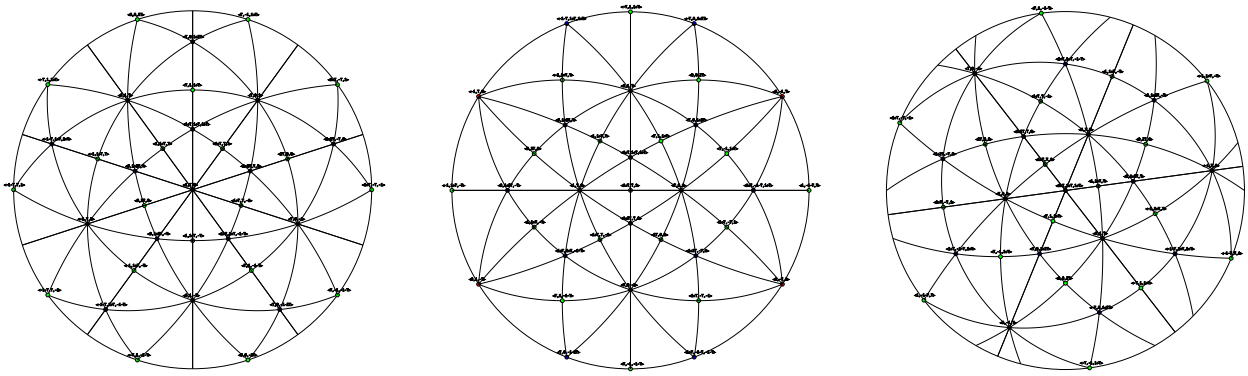

Fig. 2. Stereographic projections of the icosahedral group $m35$ along (from left to right) the 5-, 2- and 3-fold directions.

subspaces as given in Fig. 3. Then, the matrix $\widehat{\boldsymbol{M}}$ is defined[2] by the elements $\widehat{\boldsymbol{M}}_{\alpha,i} = \langle\alpha|\widehat{\mathbf{1}}|i\rangle = \langle\alpha|i\rangle$, $\widehat{\boldsymbol{M}}_{\bar{\alpha},i} = \langle\bar{\alpha}|\widehat{\mathbf{1}}|i\rangle = \langle\bar{\alpha}|i\rangle$, properly normalized by $\kappa = 1/\sqrt{2(2+\tau)}$.

Now, designating by A the lattice parameter of the hyper-cubic 6D unit cell and Λ the 6D lattice, the reciprocal lattice Λ^* has inverse parameter $1/A$. Let Q be a reflection of the primitive 6D lattice Λ that we note $P^*(1)$, $Q = (n_1, n_2, \ldots, n_6)$ and let $q_\parallel$ and $q_\perp$ be its projections in respectively $\mathbf{E}^*_\parallel$ and $\mathbf{E}^*_\perp$. Using the matrix $\widehat{\boldsymbol{M}}$, we obtain $q_\parallel = A^*\kappa(h+h'\tau, k+k'\tau, \ell+\ell'\tau)$ and $q_\perp = A^*\kappa(h'-h\tau, k'-k\tau, \ell'-\ell\tau)$, where h, h', k, k', ℓ and ℓ' are integers given by $h = n_1 - n_4$, $h' = n_2 + n_5$, $k = n_3 - n_6$, $k' = n_1 + n_4$ and $\ell = n_2 - n_5$, $\ell' = n_3 + n_6$. In Cahn et al.'s [19] notations, a 6D reflection can be noted $Q = (h/h', k/k', \ell/\ell')$, where the symbol a/b means $a + b\tau$ in $\mathbf{E}_\parallel$ and $b - a\tau$ in $\mathbf{E}_\perp$.[3] Also, the two numbers N and M defined by $N = h^2 + h'^2 + k^2 + k'^2 + \ell^2 + \ell'^2$ and $M = h'^2 + k'^2 + \ell'^2 + 2(hh' + kk' + \ell\ell')$ give the lengths of the projections of Q in $\mathbf{E}_\parallel$ and $\mathbf{E}_\perp$:

$$Q^2 = A^{*2}N/2, \qquad q_\parallel^2 = \kappa^2 A^{*2}(N + M\tau), \qquad q_\perp^2 = \kappa^2 A^{*2}\tau(N\tau - M) \tag{1}$$

Therefore, observing that $N > 0$, $q_\parallel^2 \leqslant Q^2$ and $q_\perp^2 \leqslant Q^2$, one finds that M is bounded by $-\lfloor N/\tau \rfloor \leqslant M \leqslant \lfloor N\tau \rfloor$. Thus the most intense reflections, corresponding to the smallest possible values of $|q_\perp|$—as will be made clear in the next section—are those having the M value equal to $M = \lfloor N\tau \rfloor$.[4]

[2] It is interesting to note that $\widehat{\boldsymbol{M}}^{-1} = {}^t\widehat{\boldsymbol{M}}$, so that, backwards, a ket $|U\rangle$ in $\mathbf{E}_\parallel$, with internal coordinates (x, y, z) on the $\{|\alpha\rangle\}$ basis, has on the canonical $\{|i\rangle\}$ basis, the *six* coordinates $\kappa(x+\tau y, \tau x+z, y+\tau z, -x+\tau y, \tau x-z, -y+\tau z) \in \mathbf{E}^6$. Similarly, a ket $|V\rangle$ in $\mathbf{E}_\perp$ with internal coordinates (x', y', z') on the $\{|\bar{\alpha}\rangle\}$ basis has, expressed on the canonical basis $\{|i\rangle\}$, the *six* coordinates $\kappa(-\tau x' + y', x' - \tau z', -\tau y' + z', \tau x' + y', x' + \tau z', \tau y' + z') \in \mathbf{E}^6$.

[3] For example, the reflection $Q = (1/1, 2/1, 1/2)$ projects in $\mathbf{E}_\parallel$ and $\mathbf{E}_\perp$ according to respectively $q_\parallel = A^*\kappa(1+\tau, 2+\tau, 1+2\tau)$ and $q_\perp = A^*\kappa(1-\tau, 1-2\tau, 2-\tau)$.

[4] The experimental observation in the powder diffraction patterns that the strong reflections occurred indeed at distances $q_\parallel = \kappa A^*\sqrt{N + \lfloor N\tau \rfloor \tau}$ has been a very important success for the cut and projection description.

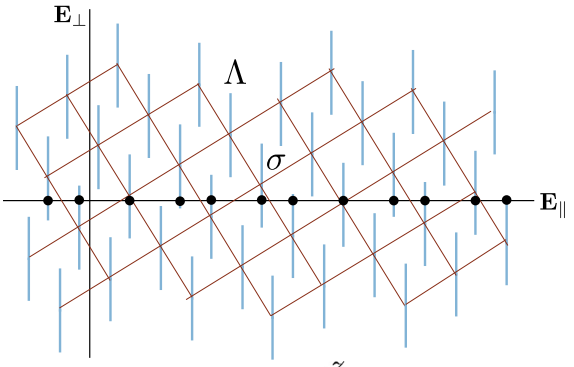

	$\widehat{\mathbf{1}}$	$(\widehat{\mathbf{5}},\widehat{\mathbf{5}}^4)$	$(\widehat{\mathbf{5}}^2,\widehat{\mathbf{5}}^3)$	$\widehat{\mathbf{2}}$	$(\widehat{\mathbf{3}},\widehat{\mathbf{3}}^2)$
A_1	1	1	1	1	1
Γ_3	3	τ	$1-\tau$	-1	0
$\Gamma_{\bar{3}}$	3	$1-\tau$	τ	-1	0
Γ_4	4	-1	-1	0	1
Γ_5	5	0	0	1	-1
Γ_6	6	1	1	-2	0

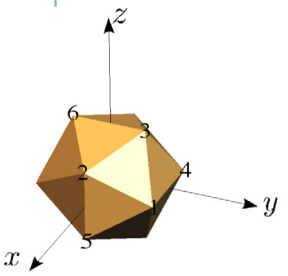

$\mathbf{E}_\parallel$

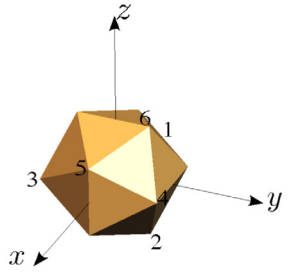

$\mathbf{E}_\perp$

$\langle\alpha\vert i\rangle$	1	2	3	4	5	6
x	1	τ	0	-1	τ	0
y	τ	0	1	τ	0	-1
z	0	1	τ	0	-1	τ

$\langle\bar{\alpha}\vert i\rangle$	1	2	3	4	5	6
x'	$-\tau$	1	0	τ	1	0
y'	1	0	$-\tau$	1	0	τ
z'	0	$-\tau$	1	0	τ	1

Fig. 3. (Color online.) On top: Principle of the cut (and project) method (see text). On the left: the character table of group 235 (group *I*) of the icosahedron. The representation Γ_6 is the sum of the irreducible representations Γ_3 and $\Gamma_{\bar{3}}$. On the right: the components $\langle\alpha|i\rangle$ of the projection of the 6D unit vectors as defined on the drawing, on $\mathbf{E}_\parallel$, and $\langle\bar{\alpha}|i\rangle$ on $\mathbf{E}_\perp$.

There are *three* Bravais icosahedral classes in the 6D space[5]:

(i) simple hypercubic $P(1) = (n_1, n_2, \ldots, n_6)$, with $n_i \in \mathbb{Z}$;
(ii) face centered hypercubic with lattice parameter $2A$ noted $F(2) = (n_1, n_2, \ldots, n_6)$, such that $\sum n_i$ is even;
(iii) centered hypercubic with lattice parameter $2A$ noted $I(2) = (n_1, n_2, \ldots, n_6)$, all n_i have the same parity.

The numbers N and M are very convenient to characterize these three Bravais lattices. Indeed, it is easily verified that $N = h + k' \bmod 2$ and $M = h' + k' + \ell' \bmod 2$ so that we have (see Fig. 4):

(i) $F(2)$ (reciprocal $I(1)$) N, M no conditions;
(ii) $P(1)$ (reciprocal $P(1)$) N even, M no condition;
(iii) $I(1)$ (reciprocal $F(2)$) N even, M even.

2.2. Diffraction

Diffraction is the fundamental experimental tool for quasicrystal atomic structure determination. The diffraction pattern of a quasiperiodic structure is the Fourier transform:

$$F(q_\parallel) = \sum_j f_j(q_\parallel) \mathrm{e}^{2\mathrm{i}\pi q_\parallel . r_\parallel^j}$$

where j designates the atom located at position $r_\parallel^j$ and $f_j(q_\parallel)$ its atomic form factor.

Let us consider for simplicity that the structure is made of one single kind of atom α, generated by the cut method using one unique atomic surface (AS) A_α centered at the nodes of the hyperlattice Λ. Because the structure is quasiperiodic, the positions $r_\parallel^j$ are the projection in $\mathbf{E}_\parallel$ of certain nodes λ^j of the hyperlattice:

[5] The lattices $F(2)$ and $I(2)$ of lattice parameters $2A$ are sublattices of $P(1)$ with indices $P(1) : F(2) = 2$ and $P(1) : I(2) = 32$. It is more interesting to consider $I(1)$ instead of $I(2)$ with then the general group subgroup relation $F(2) \in P(1) \in I(1)$ of index 2 at each step for any finite dimension.

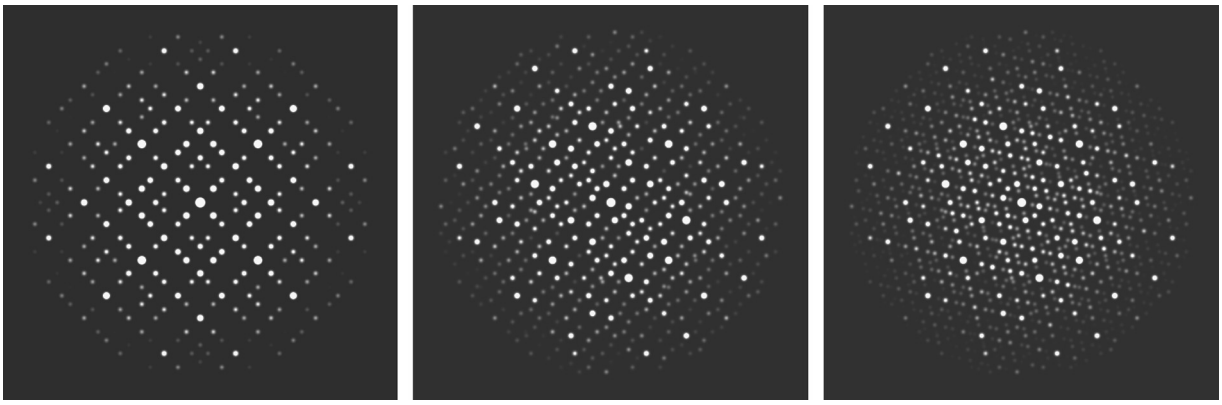

Fig. 4. 2-fold diffraction plane for I-, P- and F-type icosahedral structures (I-type structures have so far never been observed).

$$\varrho_j = \left(\bigcup_{\lambda^j \in \Lambda} \sigma_\lambda^j \right) \cap \mathbf{E}_\parallel$$

and thus $r_\parallel^j + r_\perp^j = \lambda^j$, where the component $r_\perp^j$ projects in $\mathbf{E}_\perp$ inside the atomic surface A_α located at λ^j. If $q_\parallel$ is a generic wave vector, then the phases in the exponential of the Fourier transform fill uniformly the unit circle and the resulting diffracting wave in the $q_\parallel$ direction vanishes. But, if $q_\parallel$ is the projection in $\mathbf{E}_\parallel$ of a wave vector of the reciprocal lattice Λ^*, $q_\parallel + q_\perp = Q$, then the argument in the exponential can be written as:

$$q_\parallel . r_\parallel^j = Q . \lambda - q_\perp . r_\perp^j = -q_\perp . r_\perp^j \bmod 1;$$

and thus:

$$F(q_\parallel) = f_\alpha(q_\parallel) \sum_j \mathrm{e}^{2\mathrm{i}\pi q_\parallel . r_\parallel^j} = f_\alpha(q_\parallel) \sum_j \mathrm{e}^{-2\mathrm{i}\pi q_\perp . r_\perp^j}, \quad \text{with } \lim_{j\to\infty} \sum_j \mathrm{e}^{-2\mathrm{i}\pi q_\perp . r_\perp^j} = \int_{r_\perp \in A_\alpha} \mathrm{e}^{-2\mathrm{i}\pi q_\perp . r_\perp} \, \mathrm{d}V_\perp$$

Here we make explicit use of the fact that the projections in $\mathbf{E}_\perp$ of the nodes of Λ form a dense set of point and we select only those projecting inside A_α.

Generalizing this formula to an arbitrary number of atomic species and atomic surfaces leads to:

$$f(q_\parallel) = \sum_j^P f_j(q_\parallel) \eta_j(q_\perp) \mathrm{e}^{2\mathrm{i}\pi Q \cdot R_j} \quad \text{with } \eta_j(q_\perp) = \int_{r_\perp \in A_j} \mathrm{e}^{-2\mathrm{i}\pi q_\perp . r_\perp} \mathrm{d}V_\perp \tag{2}$$

where P is the number of ASs defining the structure in the elementary 6D-unit cell, $f_j(q_\parallel)$ the atomic form factor of the chemical species associated with the j-th AS, $\eta_j(q_\perp)$ the Fourier transform of the characteristic functions of the AS that takes value 1 inside the AS and 0 outside, and R_j the locations of the ASs in the unit cell in the hyperspace.

For specific R_j with simple rational coordinates, the phase factors $\mathrm{e}^{2\mathrm{i}\pi Q \cdot R_j}$ take simple values and the global structure factors can be written as additions and/or subtractions of the scatterers issued from the various ASs as shown in Fig. 5. Indeed, an AS located at R is reproduced by symmetry at all other equivalent sites on the unit cell, the number of which is given by the order of the little group of R, say G_R into the point group, say G, of the quasicrystal: $\nu = |G|/|G_R|$. The set of equivalent vectors is defined by the coset decomposition of G onto G_R, $G = \bigcup_{i=1}^{\nu} g_j G_R$, and given by the collection of the ν vectors $g_j R$. The global phase factor $Y(Q)$ attributed to one AS located at R is therefore:

$$Y(Q) = \frac{1}{\nu} \sum_{j=1}^{\nu} \mathrm{e}^{2\mathrm{i}\pi Q \cdot g_j R}$$

and the general formula for calculating the diffracted intensities of quasicrystals finally writes:

$$f(q_\parallel) = \sum_j^P f_j(q_\parallel) \eta_j(q_\perp) Y(Q) \tag{3}$$

where the sum over j runs on the different atomic orbits of the structure.

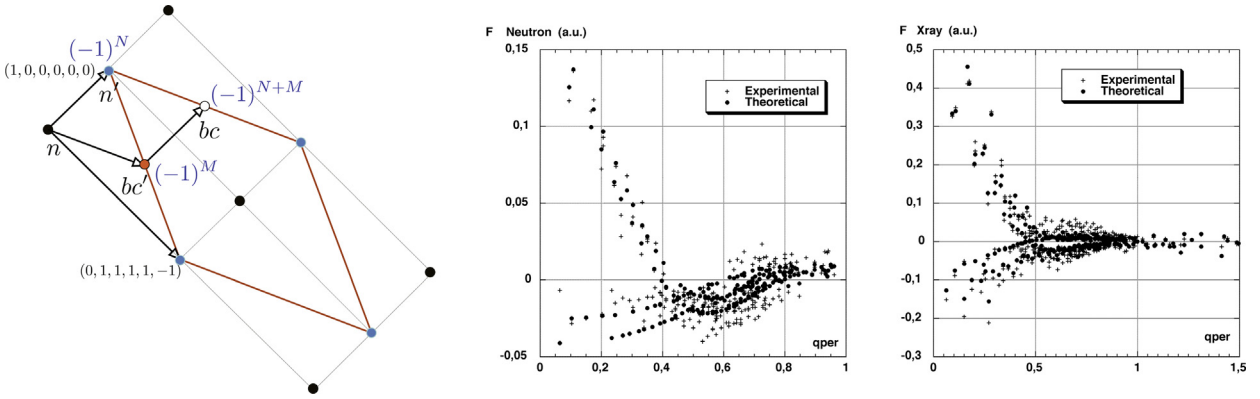

Fig. 5. (Color online.) Locating atomic surfaces at high symmetry points $R = \{n, n', bc, bc'\}$ of the hyperlattice Λ generates phases shifts between diffraction beams that are directly correlated with the parity of N and M, as shown on the left. On the right, the experimental data on AlCuFe (courtesy of Quiquandon et al. [20]) show that the diffraction beams indeed split into four families according to the parity of N and M.

2.3. Atomic surfaces

The atomic surfaces that generate the term $\eta_j(q_\perp)$ in the diffraction expression (3) are bounded volumes that we assume to be *piecewise parallel* to $\mathbf{E}_\perp$ for the following physical reasons.

- This first geometrical constrain is introduced for *structural simplicity*: like in usual crystals, we ask the structure to show *finite local complexity* in the sense that each type of atom should have a finite number of different local environments to any finite size.[6] The property of finite local complexity makes possible the description of the atomic structure by the knowledge of all the possible atomic local environments, also called the *atlas* of the atomic configurations together with their occurrence frequencies. Under this requirement of *finite local complexity*, quasiperiodic atomic structures share many properties with quasiperiodic tilings that appear as underlying skeletons of the atomic structures, like lattices for regular crystals.
- The second requirement is based on the idea that quasicrystals are considered as belonging to the possible structural solutions that solids can take at low temperature for minimizing their internal energy. Indeed, archetypal tilings are known that have local matching rules[7] and can therefore be viewed as possible ground states for some hypothetical finite range interaction Hamiltonians. Works on matching rules in tiling theory have been very intensive in the 1990s (see for instance [21–24]). Their existence is closely related to the way the cut space intersects rational (hyper)-planes family sustained by the N-dim lattice that should never be crossed by $\mathbf{E}_\parallel$. These forbidden planes must be numerous enough for forcing the cut space to be oriented in a unique way. Forbidden planes for the icosahedral case are mirror planes of $m35$ and matching rules can be found in tilings generated by ASs bounded by mirror planes, *i.e.* polyhedra that are also a good way to increase the compacity of the model.
- The third and last constrain comes from the fact that it has been early recognized that matching rules are not growth rules, since the growth process is fundamentally non-local. The real structures grow from melt of the alloys and present a strong quasicrystalline perfection. We therefore assume that the atomic jumps necessary to locally recover the ideal quasiperiodic stacking should be of very low energy. This means that these jumps occur on small or very small distances. This is the aim of the *closeness condition*[8] that is satisfied for polyhedral ASs with vertices located in $\mathbf{E}_\perp$ on points that are rationally scaled with respect to the $\mathbb{Z}$-module of the projected hyper-lattice.

All together, these constrains suggest constructing AS for the icosahedral phase as polyhedra resulting from intersections, unions and/or rescaling by any number of the form $(n + m\tau)/d, n, m \in \mathbb{Z}, d \in \mathbb{N}^+$ of the eight bounded polyhedra defined by the elementary tessellation under the point group $m35$ (or any subgroup of $m35$) of the mirror planes perpendicular to the 2-fold axes and shown in Fig. 6.

[6] This requirement is not fulfilled in incommensurate structures and could be one of the *distingo* between quasicrystals and incommensurate phases.

[7] We say that a tiling has matching rules if there exists a set of local constrains that enforce quasiperiodicity of the tiling as soon as they are satisfied everywhere in the tiling.

[8] For allowing an easy bulk reconstruction, the cut should easily "glide" in the 6D space along $\mathbf{E}_\perp$ in exploring the class of the indistinguishable structures through low-energy atomic jumps with no transport of matter at long distances.

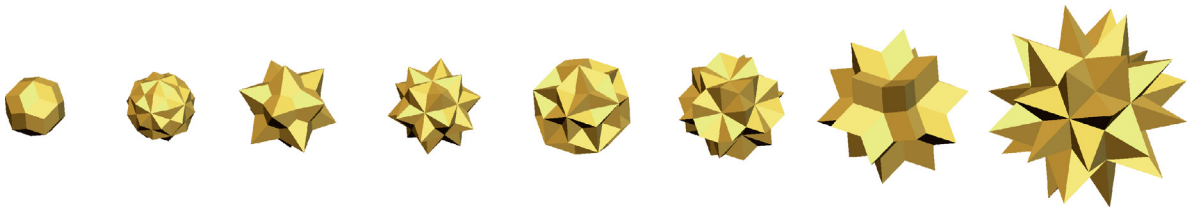

Fig. 6. (Color online.) Tessellations of the triacontahedron with normals to facets along the 2-fold directions. All these forms and their intersections can be used to generate the ASs of the models of real icosahedral quasicrystals after [20]).

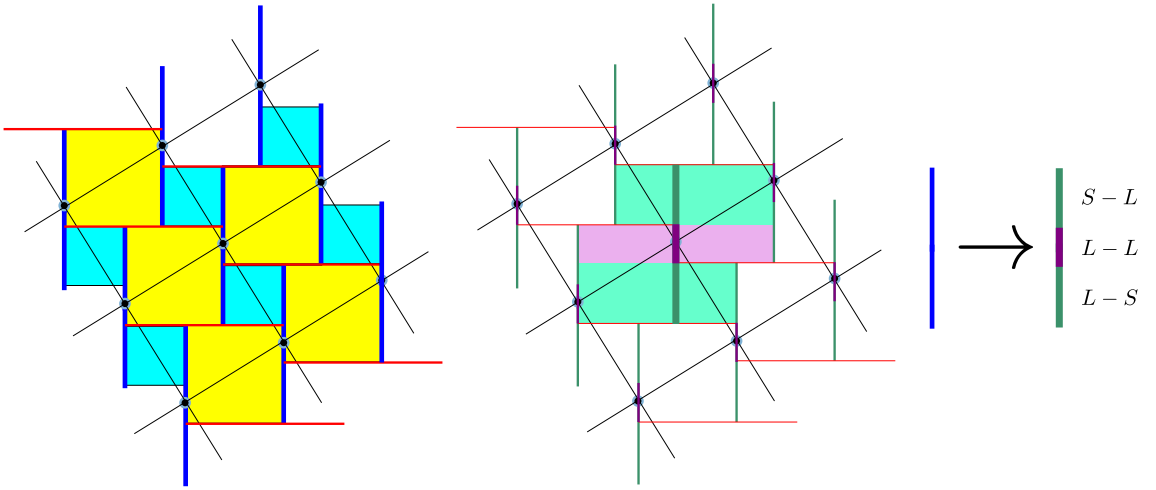

Fig. 7. A 1D quasiperiodic chain of S and L segments generated by the ASs represented in dark blue. Two consecutive segments are either $L-S$ (or $S-L$) or $L-L$ but never $S-S$, because any cut hits either a yellow and a blue squares or two yellow squares, but never two consecutive blue squares. The AS can therefore be decomposed into two cells: the purple cell at the center that generates all points that have a long segment on both sides, and the green cell that generates the points that have a long segment on one side and a short on the other one. (For interpretation of the references to color in this figure, the reader is referred to the web version of this article.)

2.4. The cell decomposition

One of the most powerful features of the cut method is that all geometrical properties of the quasicrystal can be derived from the examination of a unique finite size unit cell of the periodic object in the hyperspace. For example, the composition and the density of the quasicrystal are directly obtained by the knowledge of the volumes of the atomic surfaces in $\mathbf{E}_\perp$.

More interestingly, the atomic configurations of the quasicrystals can be directly analyzed using the cell decomposition technique. Consider, for example, the simple case of a 1D quasiperiodic sequence of S and L segments generated by the AS drawn in blue in Fig. 7. By connecting the neighboring ASs, we obtain a new decomposition of the 2D unit cell into subcells with boundaries parallel to $\mathbf{E}_\parallel$ (horizontal) and $\mathbf{E}_\perp$ (vertical). They are two squares, a yellow one and a blue one. Each time, $\mathbf{E}_\parallel$ hits a yellow square, an L segment is generated, each time it hits a blue square, an S segment is generated. Thus the relative number of S to L segments is given by the ratio of the edges of the squares (generally the surfaces of the facets of the cells along $\mathbf{E}_\perp$). Also two blue squares are never adjacent; thus they are no $S-S$ sequences in the tiling and the relative number of $S-L$ ($L-S$) versus $L-L$ sequences is given by the width along $\mathbf{E}_\perp$ of the purple rectangle versus the one of the green rectangle as drawn in the middle of Fig. 7. Associating A and B atoms with the purple and green atomic cells, respectively, generates a quasiperiodic chain with two kind of atoms: atoms A are surrounded by L segments on both sides and atoms B have an S segment on one side and an L segment on the other one. The chemical species A and B are distributed there on the quasiperiodic chain in a way that atoms of the same species have the same *local* (here to first neighbor distance L) environment.

More generally, the cell decomposition consists in projecting all ASs in $\mathbf{E}_\perp$ along $\mathbf{E}_\parallel$ that are inside a ball of finite radius R around a chosen AS taken as origin. This makes a partitioning of the AS into cells, where *each cell corresponds to a certain arrangement of the surrounding atoms up to distance R*. In the previous example, we showed that at radius $R = L$ they are two different local arrangements around a central atom: $S-L$ ($L-S$) or $L-L$, defined by the two different cells shown on Fig. 7.

3. Atomic structures of the icosahedral phases

Beyond the F-type archetypal icosahedral phases like i-AlPdMn and i-AlCuFe that have been widely studied (see for instance [25,26,20,27–29]), A.-P. Tsai [30] and his group have recently discovered new icosahedral phases of type $P(1)$ in

binary and ternary metallic systems, as (Cd, Yb) and (Zn, Mg, RE, RE = rare earth), which complete the archetypal structures (see the article by C. Pay Gomez and A.P. Tsai, this issue and [31,32]).

As in standard crystallography, we assume that the locations of the diffraction peaks are given by the experiments and cannot be moved. This fixes the lattice Λ and the subspaces $\mathbf{E}_\parallel$ and $\mathbf{E}_\perp$. Symmetry requirements—here icosahedral symmetry—lead to unique solutions with no possible adjustable parameters. Thus, the remaining possible fit variables are the number of ASs, their positions and shapes and the distribution of the chemical species in their decomposition cells.

All icosahedral quasicrystals recognized so far share the basic property of being described by few high symmetry ASs located on special points of their hyperspace group.

For example, the first analysis of M. Cornier-Quiquandon et al. [20] of the F-type i-AlCuFe—which applies as well for the F-type i-AlPdMn as shown by M. Boudard et al. [27,28]—shows that the diffracted intensities distribute in four branches when plotted as a function of $|q_\perp|$, as shown in Fig. 5. Each branch is characteristic of the parity of the two integers N and M discussed in the previous section. This splitting into four families is the signature of the structures of i-AlCuFe and i-AlPdMn, being primarily made of three or four ASs located at the special points $n = (0,0,0,0,0,0)$, $n' = (1,0,0,0,0,0)$ and $bc = 1/2(\bar{1},1,1,1,1,\bar{1})$ and possibly $bc' = 1/2(1,1,1,1,1,\bar{1})$. Moreover, using the fact that the characteristic functions $\eta(q_\perp)$ are positive values for small $|q_\perp|$ (converging to the value of the volume of the corresponding AS for $|q_\perp| \to 0$), a simple examination of the experimental intensities leads to assert that there are two large ASs at n and n' (the largest on n) and one or two small at bc and/or bc'. Additional small ASs are often suspected at the mid-edges $1/2(1,0,0,0,0,0)$. Because they have small volumes and do not seem to play an important role in the main features of the structures, we will not consider them here.

3.1. The general framework

A first basic requirement for modeling the atomic structure is to use ASs large enough to fit the experimental density. An order of magnitude is to consider that an atom occupies roughly 0.015 nm^3. Hence the density d of nodes should be in the order of $d \approx 66$ nm^{-3}. The length unit in $\mathbf{E}_\perp$ being arbitrary, we scale the volume of the canonical triacontahedron, that is the convex hull of projection in $\mathbf{E}_\perp$ of the 6D primitive unit cell, to the dimensionless value of $(2\tau + 1)$. In that unit, the density of atom sites per nm^3 in real space is given by:

$$\boxed{dA^3 = \frac{\nu}{\kappa(\tau+1)} V_t} \tag{4}$$

where A is the 6D $P(1)$-lattice parameter expressed in nm, ν takes values 1/2, 1 or 2 for respectively $F(2)$, $P(1)$ and $I(1)$ 6D-lattice types, and V_t is the total volume of the ASs in the 6D unit cell. Thus, the total volume of the ASs is close to $dA^3\kappa(\tau+1)/\nu$, or $66/\nu\ A^3$ per primitive unit cell as drawn on the left-hand side of Fig. 8. For example, one finds $V_t \approx 16.6$ for the F-type phase of i-AlCuFe with parameter $A = 0.63146$ nm and $V_t \approx 17.5$ for i-AlPdMn, of parameter $A = 0.645$ nm. For larger parameters, like in i-CdY primitive structures with $A = 0.75$ nm, the total ASs volume jumps to $V_t \approx 27.8$, which clearly shows these last $P(1)$-structures should be described with ASs significantly different from those used for the previous $F(2)$ structures.

For the range of A parameters between 0.6 to 0.8 nm, finding simple and large enough ASs for both the $F(2)$ and $P(1)$ structures is relatively easy. To reach a reasonable density, the canonical triacontahedron should be enlarged by a (linear) factor τ and will be designed here as T_n. The first short distances are observed along the 5f- and 3f-directions:

- in the 5f-direction:
  - $(n - n') : (-2,1,1,1,1,-1)\ \sqrt{18-11\tau}\ (0.1669\ A)$
  - $(n' - bc) : (1,1,-3,1,-1,1)/2\ \sqrt{7-4\tau}\ (0.2701\ A)$
- in the 3f-direction:
  - $(n - bc) : (-3,1,1,3,3,1)/2\ \sqrt{15-9\tau}\ (0.2459\ A)$

Thus, for A parameters smaller than 0.75 nm, all three distances are too short for being physically acceptable, but for parameters around and above this value, the distance $n' - bc$ along the 5f-direction becomes acceptable. This will lead to two possible sets of ASs according to the value of A between roughly 0.6 and 0.8 nm.

Locating T_n at each node of the $P(1)$ underlying lattice generates anyway unacceptable short atomic distances $n - n'$ along the 5-fold direction between two T_n displaced by $(\bar{2}11111)$. Because $F(2)$ structures differentiate the nodes $n = (000000)$ and $n' = (1,0,0,0,0,0)$, the T_n at the odd nodes are truncated by the traces of the T_n displaced by $(\bar{2}11111)$ from them. This leads to choose ASs at n' that are slightly smaller than those at n, as shown in Fig. 8. Concerning the $P(1)$ structures, the same ASs must be used for n and n'. Thus, the previous T_n at n and $T_{n'}$ at n' are replaced by the polyhedron T_H introduced long ago by C. Henley and V. Elser [15]. It is obtained by distributing equally the previous truncation on the two even and odd triacontahedra. It has the same vertices as $T_{n'}$ except the vertex along the 5-fold direction that is the $(\mathbf{E}_\perp)$ projection of the middle of the vector $(\bar{2}11111)$, as shown in Fig. 8. At that stage, $F(2)$ and $P(1)$ structures have the very same density of nodes: $V_n = 5 + 8\tau$, $V_{n'} = 5 + 6\tau$ for $F(2)$ and $V_n = 5 + 7\tau$ for $P(1)$. Using these basic ASs and taking into account the two other small distances, we end up as seen on Fig. 8 with:

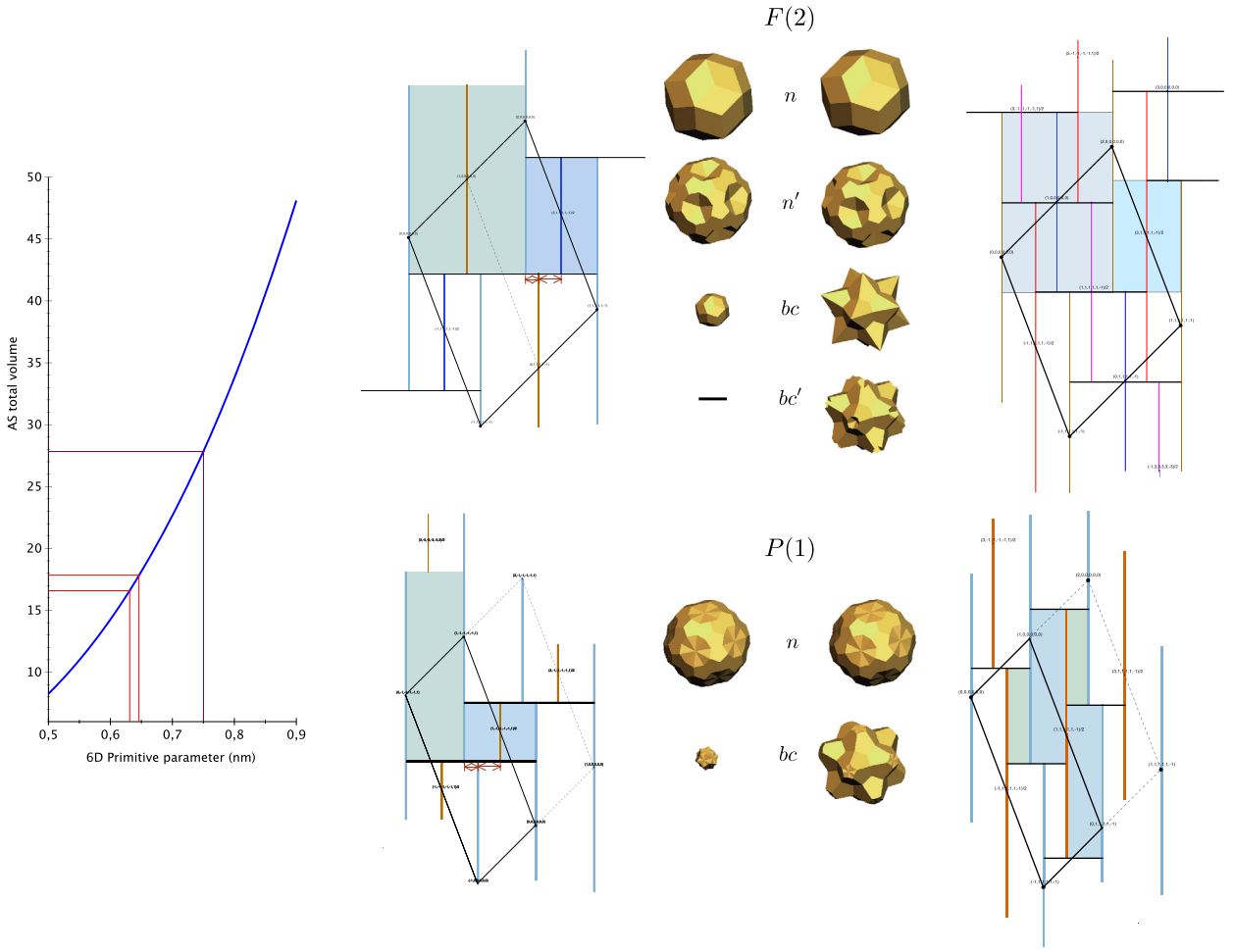

Fig. 8. Left: variation of the total ASs volumes as a function of the 6D lattice parameter. Middle and the right: simplest ASs located at the special points n, n', bc and bc' that can be used to describe the $F(2)$ (top) and $P(1)$ (bottom) icosahedral structures as a function of the 6D primitive lattice parameter: i-AlCuFe and i-AlPdMn have 6D lattice parameters around 0.64 nm (red lines in the plot on the left) corresponding to atomic surfaces with a total volume around 17 per primitive unit cell (left column of the $F(2)$ and $P(1)$), whereas CdY-type phases have 6D lattice parameters around 0.75 nm, with atomic surfaces of total volume around 27 per primitive unit cell shown on the right column of the $F(2)$ and $P(1)$ structures. Critical short distances are visualized as red arrows on the rational 6D cuts along the 5-f 2D-planes. (For interpretation of the references to color in this figure, the reader is referred to the web version of this article.)

- a set S_1 for small A parameters, with either a small triacontahedron at bc and no AS at bc' for the $F(2)$ structure or a smaller volume at bc for the $P(1)$ structure;
- a set S_2 for large A parameters, the ASs located at $bc(bc')$ are much larger in both cases, as seen in Fig. 8.

The first set S_1 has a total ASs volume per primitive unit cell of $(11+14\tau)/2 = 16.826_2$ for $F(2)$ and $(77+106\tau)/15 = 16.56_7$ for $P(1)$. The second set S_2 leads to $10+9\tau = 24.56_2$ for $F(2)$ and $(103+164\tau)/15 = 24.55_7$ for $P(1)$.

An evident first conclusion of these basic features is that there are very little differences between F and P structures. Indeed, $F(2)$ structures can be conveniently described using the $P(1)$ set of ASs, but assigning different atomic species and cell decompositions on the even and odd nodes: thus, assigning the same chemical decoration on even and odd nodes leads to a $P(1)$-type structure, whereas distributing the atomic species differently between even and odd nodes eventually leads to an $F(2)$ structure. In that simple scheme, both $P(1)$ and $F(2)$ structures share the same kind of geometric atomic clusters, but differ in their chemical decorations at even and odd nodes.

The two basic sets presented here are simple primary tools to model ASs in icosahedral phases. Many variations can be done starting from them. One consists in enlarging one chosen AS and depleting the other ones that would then generate too short distances with it. This is what is done for generating Mackay clusters, as it will be seen in the next section. A second variation consists in allowing a displacement shift of the atoms of an orbit in $\mathbf{E}_\parallel$ consistently with the local symmetry out of the theoretical positions given by the cut and project. This is the case for generating Mackay and Tsai clusters corresponding to the actual clusters experimentally identified in periodic approximants of the icosahedral phases (see P. Guyot and M. Audier, this issue, and [34–36] for the Tsai cluster).

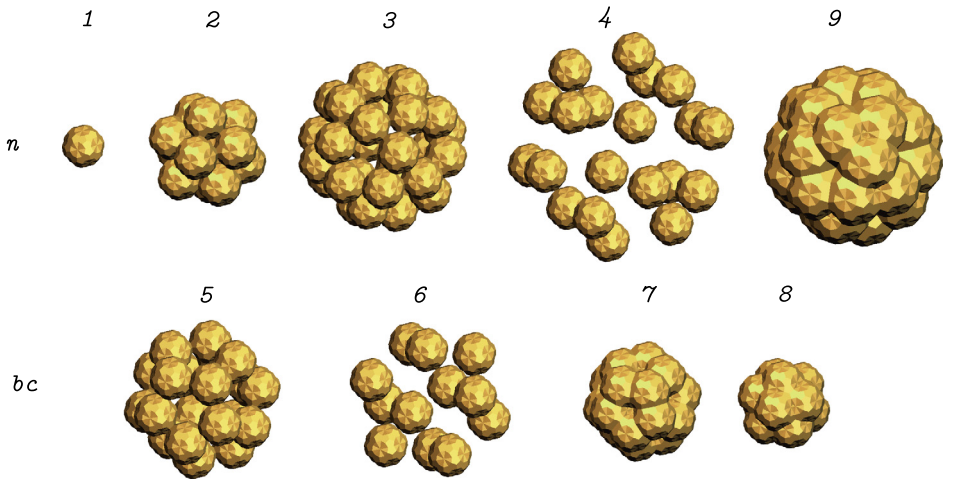

Fig. 9. (Color online.) ASs at $n(n')$ and $bc(bc')$ that generate the various orbits of atomic clusters around the center irrespective of the possible generation of (too) short atomic distances. ASs (see Fig. 8) used for building ACs in the icosahedral phases. The ASs T_4 and T_6 extend outside the basic ASs seen on Fig. 8 for both sets 1 and 2. They can be used either with partial occupancy factors or in removing the intersection cells from the main large ASs. Polyhedra T_1 to T_6 are those introduced by Takakura et al. [33] to characterize the atomic structure of i-CdY.

Table 1
The main first plausible interatomic distances and their corresponding symmetries are translations in 6D-space. The distances are given in units of KA, where $K = 1/\sqrt{2(2+\tau)} (\approx 0.371748)$ is the geometric constant introduced by Cahn et al. [19] and in A units (in bold, the lines that define the ASs shown in Fig. 9).

AS	type	sym(lattice)	6D-vector	$d_\parallel$ (in KA unit)	$d_\parallel$ (in A unit)
T_1	**n**	**1(F)**	$(\mathbf{0},\mathbf{0},\mathbf{0},\mathbf{0},\mathbf{0},\mathbf{0})$	$\mathbf{0}$	**0.0**
–	bc'	$12(I)$	$(-1,-1,3,-1,1,-1)/2$	$\sqrt{7-4\tau}$	0.2701
T_4	**n′**	**20(P)**	$(\mathbf{1},\mathbf{0},\mathbf{0},-\mathbf{1},-\mathbf{1},\mathbf{0})$	$\sqrt{\mathbf{6-3\tau}}$	**0.3980**
T_6	**bc**	**12(I)**	$(\mathbf{1},\mathbf{1},-\mathbf{1},\mathbf{1},-\mathbf{1},\mathbf{1})/\mathbf{2}$	$\sqrt{\mathbf{3}-\tau}$	**0.4370**
T_5	**bc′**	**20(I)**	$(-\mathbf{1},\mathbf{1},\mathbf{1},\mathbf{1},\mathbf{1},\mathbf{1})/\mathbf{2}$	$\sqrt{\mathbf{3}}$	**0.6439**
T_2	**n′**	**12(P)**	$(\mathbf{0},\mathbf{0},\mathbf{1},\mathbf{0},\mathbf{0},\mathbf{0})$	$\sqrt{\mathbf{2}+\tau}$	**0.7071**
T_3	**n**	**30(F)**	$(\mathbf{0},\mathbf{1},\mathbf{0},\mathbf{0},-\mathbf{1},\mathbf{0})$	$\mathbf{2}$	**0.7435**
–	bc	$60(I)$	$(1,-1,1,1,1,3)/2$	$\sqrt{7-\tau}$	0.8624
–	n'	$60(P)$	$(0,1,0,1,0,1)$	$\sqrt{6+\tau}$	1.0261
T_7	**bc**	20(**I**)	$(\mathbf{1},\mathbf{1},\mathbf{1},-\mathbf{1},-\mathbf{1},\mathbf{1})/\mathbf{2}$	$\sqrt{\mathbf{3+3\tau}}$	**1.0419**
T_8	**bc′**	**12(I)**	$(\mathbf{1},\mathbf{1},\mathbf{1},\mathbf{1},-\mathbf{1},\mathbf{1})/\mathbf{2}$	$\sqrt{\mathbf{3+4\tau}}$	**1.1441**
–	n	$60(F)$	$(1,0,1,-1,-1,0)$	$2\sqrt{2}$	1.0515
T_9	**n**	**30(F)**	$(\mathbf{0},\mathbf{0},\mathbf{1},\mathbf{0},\mathbf{0},\mathbf{1})$	$\mathbf{2\tau}$	**1.2030**

3.2. Atomic clusters (AC)

One of the major feature of having ASs located at special points in 6D is the existence in the structure of high-symmetry atomic clusters (*AC*). An atomic cluster is a set of atomic positions characterized by the fact that *if any one of the atoms of the AC is present in the structure, then all others of the AC are also present*.

Consider one of the centers of an AC. It is generated by a (generally small) AS, say T_0. All atoms of the AC are thus generated by ASs that contain a piece that projects along $\mathbf{E}_\parallel$ exactly on T_0 (else there would be missing atoms of the AC around certain centers, or, on the contrary, missing centers for some ACs). Thus the corresponding AS located at a site t_k of the AC is *exactly* $\widehat{\pi}_\perp T_0(t_k)$ completed by all its symmetric ones around the node t_k. Assuming that the AC is made of N orbits, each of M_N surrounding atoms are characterized by translations $\widehat{\pi}_\parallel t_k$. The global ASs, AS_{AC}, that generate the AC are obtained by the union of the projections $\widehat{\pi}_\perp T_0$ on the nodes located at t_N^k sites in 6D.

The construction of AS_{AC} is achieved by starting from T_0 that is the AS generating the center and copying it on all 6D node t_j^k corresponding to the atoms of the cluster; then, these $T_0(t_j^k)$ are projected parallel to $\mathbf{E}_\parallel$ on the initial central AS. The union of these projections form the searched AS_{AC}. Finally, AS_{AC} is copied on each hyperlattice node. Thus, a given AC around a certain center characterized by the AS T_0, is generated by the AS_{AC} defined in the following way:

$$AC = \bigcup_{j=1}^{N} \bigcup_{k=1}^{M_j} \widehat{\pi}_\parallel t_j^k \quad \leftrightarrow \quad AS_{\mathrm{AC}} = \bigcup_{j=1}^{N} \bigcup_{k=1}^{M_j} \widehat{\pi}_\perp T_0\big(t_j^k\big) \tag{5}$$

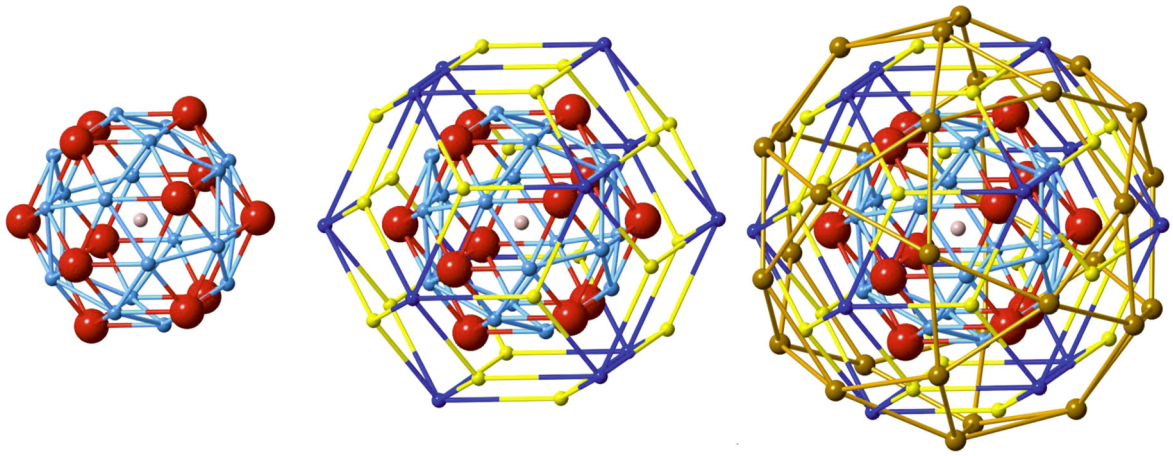

Fig. 10. Irrespective of possible unacceptable short interatomic distances, the most general cluster that can be generated in the cut method from 6D space using ASs located only on the high symmetry special points $n(n')$ and $bc(bc')$ seen in Fig. 9 is made of a center generated by T_1, an inner small triacontahedron (red and blue) generated by $T_4 \cup T_6$, a medium-size triacontahedron (yellow and dark-blue), τ times larger, generated by $T_2 \cup T_5$, and an external icosidodecahedron (brown) generated by T_3. (For interpretation of the references to color in this figure, the reader is referred to the web version of this article.)

The choice of T_0 is *a priori* arbitrary, but an optimized choice is obtained when AS_{AC} has the largest possible volume, *i.e.* when the ASs $\widehat{\pi}_\perp T_0(t_j^k)$ in (5) have the smallest intersections. For icosahedral phases, the choice of T_0 as T_H linearly rescaled by τ^{-2} shown on n in Fig. 9 is extremely efficient to insure a maximum covering on n and bc, since only T_7, T_8 and T_9 show overlaps between their cells T_0. This polyhedron appears in the cell decomposition of the canonical primitive tiling and corresponds to the centers of the high-symmetry central configuration. Fig. 9 shows the main types of ASs defined in Table 1 that are expected to be found in icosahedral phases using T_H as generator for centers.

The generic atomic cluster that can be generated using ASs located on $n(n')$ and $bc(bc')$ special points in 6D-space is shown in Fig. 10. It is built with two concentric triacontahedra and an external icosidodecahedron. Larger orbits, like those generated by T_7, T_8 and T_9, are shared between different atomic clusters.

In practice, of course, not all orbits are occupied because of the many possible short interatomic distances they generate depending on the value of the 6D primitive lattice parameter A. For example, for small A values, the first inner triacontahedron is occupied on its icosahedral orbit alone, in which case the large AS at $n(n')$ must be depleted by their intersection with T_4 (to remove the atoms on the dodecahedron). Another solution is removing T_6 from the $bc(bc')$ that leads to sectioning T_4 by the basic large ASs at $n(n')$, thus keeping only the dodecahedron orbit partially occupied with 7 over the 20 atoms (see standard simple atomic models of *i*-AlPdMn and *i*-AlCuFe in [29]). The various types of usual atomic clusters are easily found in the present general cluster. For example, Bergman clusters are generated using T_6, T_5 and T_2, Mackay clusters using T_6, T_2 and T_3 and Tsai clusters (with the exception of the inner small tetrahedron that is not contained in our generic cluster) by T_5, T_2 and T_3. Bergman and Mackay clusters require an additional rescaling of the radii of T_6 and T_2 by shrinking the radius of T_6 by $(1 - \tau/2)$ (19%).

3.3. Conclusions

We have shown here that the N-dim crystallography is an efficient and powerful way of describing the atomic structures of the icosahedral phases. All the phases actually known are complicated 3D structures of strongly intricated high-symmetry atomic clusters that become most simple once embedded in their natural 6-dim space. The main atomic surfaces are located at high symmetry special points of the 6D lattice and distributed according to two main sets for both $F(2)$ and $P(1)$ 6D-lattice type depending on the value of the 6D-primitive lattice parameter A. The mean properties of these complicated atomic structures are that they are constituted of large high-symmetry atomic clusters that aggregate and interpenetrate in a quasiperiodic fashion. These clusters are identical to those actually identified by standard crystallography in the periodic approximants of those structures that are numerous in the large family of complex intermetallic phases.

References

[1] D. Shechtman, I. Blech, Metall. Trans. 16A (1985) 1005–1012.
[2] D. Shechtman, I. Blech, D. Gratias, J.W. Cahn, Phys. Rev. Lett. 53 (1984) 1951.
[3] D. Shechtman, D. Gratias, J.W. Cahn, C. R. Acad. Sci. Paris, Ser. II 300 (18) (1985) 909–913.
[4] R. Portier, D. Shechtman, D. Gratias, J.W. Cahn, J. Microsc. Spec. Élec. 10 (2) (1985) A30.
[5] J.W. Cahn, D. Gratias, D. Shechtman, J. Met. 37 (8) (1985) A62 and A74.
[6] D. Levine, P.J. Steinhardt, Phys. Rev. Lett. 53 (1984) 2477.
[7] M. Duneau, A. Katz, Phys. Rev. Lett. 54 (1985) 2688–2691.

[8] A. Katz, M. Duneau, J. Phys. 47 (1986) 181–196.
[9] A. Katz, M. Duneau, Scr. Metall. 20 (1986) 1211–1216.
[10] P.A. Kalugin, A.Y. Kitayev, L.S. Levitov, JETP Lett. 41 (1985) 145.
[11] P.A. Kalugin, A.Y. Kitayev, L.S. Levitov, J. Phys. Lett. 46 (1985) L601.
[12] V. Elser, Acta Crystallogr. A 42 (1986) 36.
[13] V. Elser, C.L. Henley, Phys. Rev. Lett. 55 (1985) 2883–2886.
[14] V. Elser, Phys. Rev. B 32 (1985) 4892–4898.
[15] C.L. Henley, V. Elser, Philos. Mag. B 53 (1986) L59–L66.
[16] J.W. Cahn, D. Gratias, B. Mozer, J. Phys. (Paris) 49 (1988) 1225–1233.
[17] D. Gratias, J.W. Cahn, B. Mozer, Phys. Rev. B 38 (3) (1988) 1643–1646.
[18] D. Gratias, J.W. Cahn, B. Mozer, Phys. Rev. B 38 (3) (1988) 1638–1642.
[19] J.W. Cahn, D. Shechtman, D. Gratias, J. Mater. Res. 1 (1986) 13–26.
[20] M. Cornier-Quiquandon, A. Quivy, S. Lefebvre, E. Elkaim, G. Heger, A. Katz, D. Gratias, Phys. Rev. B 44 (5) (1991) 2071–2084.
[21] D. Frenkel, C.L. Henley, E.D. Siggia, Phys. Rev. B 34 (1986) 3649–3669.
[22] A. Katz, Commun. Math. Phys. 118 (1988) 263–288.
[23] P.A. Kalugin, L.S. Levitov, Int. J. Mod. Phys. B 3 (6) (1986) 877–896.
[24] L.S. Levitov, in: D.P. Di Vincenzo, P.J. Steinhart (Eds.), Quasicrystals: The State of the Art, World Scientific, Singapore, 1991, pp. 239–274.
[25] M. Cornier, K. Yu-Zhang, R. Portier, D. Gratias, in: D. Gratias, L. Michel (Eds.), International Workshop on Aperiodic Crystals, Les Houches, J. Phys. 47 (7) (1986) 447–456 (Suppl. Colloq. C3).
[26] H.A. Fowler, B. Mozer, J. Sims, Phys. Rev. B 37 (1988) 3906.
[27] M. Boudard, M. Deboissieu, C. Janot, J. Dubois, C. Dong, Philos. Mag. Lett. 64 (4) (1991) 197–206.
[28] M. Boudard, M. Deboissieu, C. Janot, G. Heger, C. Beeli, H. Nissen, H. Vincent, R. Ibberson, M. Audier, J. Dubois, J. Phys. Condens. Matter 4 (50) (1992) 10149–10168.
[29] M. Quiquandon, D. Gratias, Phys. Rev. B 74 (21) (2006) 214205-1–214205-9.
[30] A.P. Tsai, J.Q. Guo, E. Abe, H. Takakura, T.J. Sato, Nature 408 (6812) (2000) 537–538.
[31] C.P. Gomez, S. Lidin, Angew. Chem., Int. Ed. 40 (21) (2001) 4037–4039 and 3935.
[32] C.P. Gomez, S. Lidin, Phys. Rev. B 6802 (2) (2003) 024203.
[33] H. Takakura, J.Q. Guo, A.P. Tsai, Philos. Mag. Lett. 81 (6) (2001) 411–418.
[34] H. Takakura, M. Shiono, T.J. Sato, A. Yamamoto, A.P. Tsai, Phys. Rev. Lett. 86 (2) (2001) 236–239.
[35] H. Takakura, A. Yamamoto, M. Shiono, T.J. Sato, A.P. Tsai, J. Alloys Compd. 342 (2002) 72–76.
[36] H. Takakura, C. Pay Gomez, A. Yamamoto, M. de Boissieu, A.P. Tsai, Nat. Mater. 6 (2007) 58.